Graduate School ETD Form 9
(Revised 12/07)

PURDUE UNIVERSITY
GRADUATE SCHOOL
Thesis/Dissertation Acceptance

This is to certify that the thesis/dissertation prepared

By America Bethanne Newnum

Entitled
Bone Metabolism: The Role of STAT3 and Reactive Oxygen Species

For the degree of Master of Science

Is approved by the final examining committee:

Jiliang Li
Chair

James Marrs

Julie Ji

To the best of my knowledge and as understood by the student in the *Research Integrity and Copyright Disclaimer (Graduate School Form 20)*, this thesis/dissertation adheres to the provisions of Purdue University's "Policy on Integrity in Research" and the use of copyrighted material.

Approved by Major Professor(s): Jiliang Li

Approved by: Simon Atkinson 06/25/2012
Head of the Graduate Program Date

Graduate School Form 20
(Revised 9/10)

PURDUE UNIVERSITY
GRADUATE SCHOOL

Research Integrity and Copyright Disclaimer

Title of Thesis/Dissertation:

Bone Metabolism: The Role of STAT3 and Reactive Oxygen Species

For the degree of Master of Science

I certify that in the preparation of this thesis, I have observed the provisions of *Purdue University Executive Memorandum No. C-22,* September 6, 1991, *Policy on Integrity in Research.**

Further, I certify that this work is free of plagiarism and all materials appearing in this thesis/dissertation have been properly quoted and attributed.

I certify that all copyrighted material incorporated into this thesis/dissertation is in compliance with the United States' copyright law and that I have received written permission from the copyright owners for my use of their work, which is beyond the scope of the law. I agree to indemnify and save harmless Purdue University from any and all claims that may be asserted or that may arise from any copyright violation.

America Bethanne Newnum

Printed Name and Signature of Candidate

06/25/2012

Date (month/day/year)

*Located at http://www.purdue.edu/policies/pages/teach_res_outreach/c_22.html

BONE METABOLISM: THE ROLE OF STAT3 AND REACTIVE OXYGEN SPECIES

A Thesis

Submitted to the Faculty

of

Purdue University

by

America Bethanne Newnum

In Partial Fulfillment of the

Requirements for the Degree

of

Master of Science

August 2012

Purdue University

Indianapolis, Indiana

This thesis is dedicated to Daria Rancid, my best friend, daughter, and furry life partner for 15 adorable years. Your refusal to give up on life after being diagnosed with leukemia has given me more strength than your kitty brain will ever realize. I also want to dedicate this work to Sahib Ali, who not only never failed to support me during my graduate school career, but made sure that I didn't starve to death or go completely insane after I broke my leg halfway through my MS program. I also can't forget Sunday Sprinkles and Willow Pillow, who staged episodes of "WWE Kitty Smackdown" in our living room to distract and amuse me. Last but not least, my four parents, Ron Newnum, Linda Holycross, Patty Kelly, and Darrell Holycross, for their encouragement during this process.

ACKNOWLEDGEMENTS

I would like to thank Dr. Li for his patience and understanding during my unconventional graduate career, and also my committee members Dr. James Marrs and Dr. Julie Ji. I would like to thank Kevin Zhou for his invaluable help in the lab and his friendship outside the lab, and Dr. Robert Yost for the opportunity to serve as a TA for K103 lab for four wonderful semesters. Last but not least, I would like to thank Dr. Keith Condon for allowing our lab to use his facilities to process our bone samples.

TABLE OF CONTENTS

Page

LIST OF FIGURES

Figure Page

LIST OF ABBREVIATIONS

ATP	Adenosine triphosphate
BMP	Bone morphogenetic proteins
BSO	Buthionine sulfoximine
CFU-O	Colony forming units-osteoblastic
CoQ	Ubiquinone
$CoQH_2$	Reduced ubiquinone
DNA	Deoxyribonucleic acid
ETC	Electron transport chain
FAD	Flavin adenine dinucleotide
FMN	Flavin mononucleotide
FSS	Fluid shear stress
GAS	γ-interferon activation sequence
Gp130	Glycoprotein 130
IL	Interleukin
JAK/STAT	Janus kinas/signal transducer and activator of transcription
KO	Knockout
LRP5	Low-density lipoprotein receptor-related protein 5
M–CSF	Macrophage colony stimulating factor

NAD^+	Nicotinamide adenine dinucleotide
RANK	Receptor activator of nuclear factor κ B
ROS	Reactive oxygen species
SH2	Src homology 2
SIE	Sis-inducible element
STAT	Signal transducer and activator of transcription
TRAP	Tartrate resistant acid phosphatase

ABSTRACT

Newnum, America Bethanne. M.S., Purdue University, August 2012. Bone Metabolism: The Role of STAT3 and Reactive Oxygen Species. Major Professor: Jiliang Li.

Signal Transducers and Activators of Transcription 3 (STAT3), a transcription factor expressed in many cell types, including osteoblasts and osteoclasts, is emerging as a key regulator of bone mass and strength. STAT3 mutations cause a rare human immunodeficiency disease characterized by extremely elevated levels of IgE in serum that have associated craniofacial and skeletal features, such as reduced bone mineral density and recurrent pathological fractures. Our microarray data and immunohistochemical staining using a normal rat model have shown that STAT3 mRNA and protein levels markedly increase in response to mechanical loading. In addition, as indicated by STAT3 phosphorylation in MC3T3-E1 osteoblastic cells, STAT3 activity significantly increases in response to 30 to 90 minutes fluid shear stress. In order to further study the role that STAT3 plays in bone responsiveness to loading, tissue-selective STAT3 knockout (KO) mice, in which inactivation of STAT3 occurs in osteoblasts, were generated by breeding the transgenic mice in which Cre recombinase cDNA was cloned downstream of a 3.6 or 2.3 kb fragment of the rat Col1a1 promoter (Col3.6-Cre and Col2.3-Cre, respectively) with a strain of floxed mice in which the two loxP sites flank exons 18-20 of the STAT3 gene were used. Mice engineered with bone

selective inactivation of STAT3 in osteoblasts exhibited significantly lower bone mineral density (7-12%, $p<0.05$) and reduced ultimate force (21-34%, $p<0.01$) compared to their age-matched littermate controls. The right ulnae of 16-week-old bone specific STAT3 KO mice and the age-matched control mice were loaded with peak forces of 2.5 N and 2.75 N for female and male mice, respectively, at 2 Hz, 120 cycles/day for 3 consecutive days. Mice with inactivation of STAT3 specific in bone were significantly less responsive to mechanical loading than the control mice as indicated by decreased relative mineralizing surface (rMS/BS, 47-59%, $p<0.05$) and relative bone formation rate (rBFR/BS, 64-75%, $p<0.001$). Bone responsiveness was equally decreased in mice in which STAT3 is inactivated either in early osteoblasts (Col3.6-Cre) or in mature osteoblasts (Col2.3-Cre).

Accumulating evidence indicates that bone metabolism is significantly affected by activities in mitochondria. For instance, although STAT3 is reported to be involved in bone formation and resorption through regulation of nuclear genes, inactivation of STAT3 is shown to disrupt mitochondrial activities and result in an increased level of reactive oxygen species (ROS). Inactivation of STAT3 suppressed load-driven mitochondrial activity, which led to an elevated level of ROS in cultured primary osteoblasts. Oxidative stress induced by administration of buthionine sulfoximine (BSO) significantly inhibits load-induced bone formation in wild type mice. Taken together, the results support the notion that the loss-of-function mutation of STAT3 in osteoblasts and osteocytes diminishes load-driven bone formation and impairs the regulation of oxidative stress in mitochondria.

CHAPTER 1. INTRODUCTION

1.1 Bone Cells and Bone Homeostasis

There are two main types of bone: cancellous (also called trabecular or spongy) bone, and cortical, or compact, bone. Cancellous bone is weaker than cortical bone, with a higher surface area. Bone tissue has three main types of cells: osteoblasts, osteocytes, and osteoclasts. Osteoblasts are specialized bone cells that build bone by secretion of a matrix called osteoid. When osteoblasts become trapped in this material, they become osteocytes, the most abundant cells in bone. Osteocytes maintain the general metabolism of bone tissue. Osteoclasts are the third type of specialized bone cell; they mediate bone resorption. There are two main transformative processes in bone: modeling and remodeling. Bone modeling occurs when bone formation and resorption occur on separate surfaces, is responsible for gain in skeletal mass, and occurs mainly during growth. On the other hand, bone remodeling occurs continuously. Osteoclasts and osteoblasts function together in bone remodeling. In normal bone function, both osteoclasts and osteoblasts are active in a homeostasis to optimize bone health (*1*).

1.2 Ossification of the Skeleton

There are two ways that the skeleton hardens, or ossifies, during the embryonic formation of bone. The first, and by far the most common, is endochondrial ossification. In this process, a template made of cartilage is initially laid down in the shape of the bone to be made. This template will eventually be replaced by true bone. Intramembranous ossification, on the other hand, involves formation of bone directly from osteoblasts, and only takes place in rare instances (*2*).

1.3 Osteoclast Differentiation and Proliferation

Osteoclasts, the cells responsible for bone resorption, are derived from monocyte/macrophage precursors (*3*). These precursors migrate into bone, divide, and differentiate into tartrate resistant acid phosphatase (TRAP) positive cells. They then fuse to become multinucleated cells while invading the bone shaft, thus forming the bone marrow cavity (*2*).

Although osteoclasts and osteoblasts have opposite functions, osteoclast differentiation is partially regulated by osteoblasts. Osteoclast precursor cells express receptor activator of nuclear factor κ B (RANK), which interacts with RANK ligand (RANKL); RANKL is expressed on several cell types, including osteoblasts. The cytokines interleukin 6 (IL6) and IL11 have been shown to increase osteoclastogenesis and, in turn, bone resorption (*4*). Glycoprotein 130 (Gp130), a common receptor subunit for many cytokines such as IL6 and IL11, is also present on osteoblasts (*5*). Macrophage colony stimulating factor (M-CSF) derived from stromal cells also plays a role in osteoclast differentiation (*6*).

ROS derived from mitochondria have also been shown to have a role in osteoclast formation (*7*).

1.4 Mechanotransduction

Mechanotransduction plays a crucial role in physiology of many tissues including bone. The mass and architecture in bones are governed, to some extent, by adaptive mechanisms sensitive to their mechanical environment. Fluid shear stress (FSS) is generated by the movement of interstitial fluid due to mechanical stimulation (*8*). Osteoblasts as well as their precursors are stimulated to proliferate and differentiate by FSS (*9*). This FSS-stimulated osteoblast activity also activates osteogenic genes, such as Osteoprotegrin, Msx2, and Runx2 (*10*). These genes that respond to mechanotransduction are often referred to as mechanosensitive genes. A process called mechanical loading can be used to simulate exercise in mice; this stimulates bone remodeling and osteoblasts to form new bone (*11*).

1.5 Disruptions in Bone Homeostasis

When one type of cell becomes more active than the other, the homeostasis is disturbed, which can lead to disease. Osteoporosis, one of these pathological conditions, is characterized by higher osteoclast and lower osteoblast activity. These cellular events lead to lower bone mass (*1*). Due to cancellous bone being weaker and having more surface area than cortical bone, cancellous bone is more affected by osteoporosis. As previously described, RANKL is an important factor in osteoclast differentiation, and can play a key role in osteoporosis, which has led to the development of a monoclonal

antibody for use in human osteoporosis patients (*12*). On the other hand, osteopetrosis is a lowered activity of osteoclasts due to genetic factors. Although osteopetrosis is rare compared to osteoporosis, it can be very serious; the autosomal recessive form is typically lethal within the first 10 years of life (*13*).

1.6 STATS

STATs (Signal Transducers and Activators of Transcription) are cytoplasmic factors that, when activated, transcribe many genes that are necessary for widely varying cellular processes. Seven STAT genes are present in mammals: STATs 1, 2, 3, 4, 5a, 5b, and 6. The STATs function as dimers, which can be either hetero- or homodimers, and play varied roles in cellular function (*14*).

1.7 Cytosolic STAT3

Cytosolic STAT3 has various roles in the cell, and has been shown to be necessary for the development of visceral endoderm in mouse embryos. In fact, STAT3 knockout embryos begin to disintegrate at the precise time that STAT3 expression would normally begin in the embryo between 6.5 and 7.5 days (*15*). STAT3 has also been proven necessary to maintain mouse embryonic stem cells in an undifferentiated state (*16*). In a conditional knockout of STAT3 where the gene was deleted in bone marrow and endothelial cells, a condition similar to Crohn's disease was reported. All of these mice were deceased by 8 weeks. As Crohn's disease most likely has an immune component, this suggests that STAT3 plays a role in immunity (*17*). When activated by leptin,

STAT3 aids in cell survival in hippocampal neurons, and also mediates mitochondrial stabilization (*18*).

Cytosolic STAT3 is activated by phosphorylation by IL6 and various other cytokines and growth factors (*19*). This process involves activating the JAK/STAT pathway and turns on many different types of genes, of which some are vital for survival. The process of tyrosine phosphorylation of STAT3 (and other STATs) is accomplished by the Janus Kinase/Signal Transducer and Activator of Transcription (JAK-STAT) pathway. In the case of STAT3, IL6 binds to its receptor, which activates JAK1 and JAK2, which is phosphorylated on a tyrosine, residue 1138 (Y1138) (*18*). This produces a docking site where STAT3 is phosphorylated on Y705. Two phosphorylated STAT3 molecules dimerize due to interaction of Y705 with the SH2 domain on the other STAT3 molecule; the dimer then relocates to the nucleus to transcribe genes containing GAS (γ-interferon activation sequence) elements, also called SIEs (sis-inducible element), which have the DNA sequence of 5'-TT$(N)_{4-6}$AA-3' (*20*).

STAT3 interacts with many different proteins; a very important one is GRIM-19. GRIM-19 plays a role in interferon-β and retinoic acid induced cell death, promoting apoptosis. GRIM-19 is also found in the hydrophilic arm of complex I, subunit 1λ (*21*). Residues 36-72 on GRIM-19 interfere with the DNA binding and linker domains of STAT3; this suggests that GRIM-19 prevents STAT3 from binding to DNA, thus preventing the transcription of STAT3 dependent genes. This antagonizes STAT3's anti-apototic role (*19*). Due to GRIM-19 having a dual role in both the cytoplasm/nucleus and in complex I

of the electron transport chain, and the strong association of GRIM-19 and STAT3, it was thought that STAT3 might also be present in the electron transport chain. Gp130, a receptor subunit previously mentioned in connection with IL6 and IL11, typically activates STAT3 (*22*).

1.8 Diseases Associated with STAT3 Mutation

Hyper-IgE syndrome, also called Job's syndrome, is caused by mutations in the STAT3 gene. Although there are several places in the STAT3 gene that can contain mutations, the two areas in the gene that mutate the most commonly are the SH2 domain and the DNA binding domain (*23*). This disorder causes immunity and connective tissue to be abnormal, and is autosomal dominant. It also causes marked scoliosis, abnormal bone formation, and bowed legs.

1.9 Mitochondrial STAT3

Mitochondrial STAT3 was found due to the co-localization of STAT3 and GRIM-19. It was also verified that the STAT3 found was not a cytoplasmic contaminant. Mitochondrial STAT3 (mSTAT3) has been shown to be located in either the inner mitochondrial membrane or in the matrix rather than the outer mitochondrial membrane (*24*).

Specifically, mSTAT3 is located in complex I of the electron transport chain. There is also evidence to suggest that mSTAT3 is either also located in complex II of the electron transport chain, or in a location where complex I and complex II interact. This is thought

to be a possibility due to the facts that the complex II Fp subunit co-precipitates with complex I, and STAT3 knockouts have greatly diminished complex II function. Being a component of complex I in the electron transport chain, mitochondrial STAT3 plays a role in cellular respiration. The activity of complexes I and II in murine pro-B cells was decreased significantly; complexes III and IV were not affected (*24*).

Unlike cytosolic STAT3, mSTAT3 is predominantly phosphorylated on S727 rather than Y705. When compared to whole cell extracts, the ratio of total STAT3 to serine phosphorylated STAT3 was 2.5, in cytosolic extracts it was 2.3, and in mitochondrial extracts it was 0.3, indicating a strong presence of serine phosphorylated STAT3 in mitochondria. mSTAT3 is also thought to be present as a monomer instead of a dimer, due to the lack of interaction with another STAT3 molecule at the SH2 domain (*24*).

STAT3 is phosphorylated on S727 by the MAPK family of serine kinases. These recognize a conserved PMSP (Proline-Methionine-Serine-Proline) sequence on the C-terminal end of the protein. There are many MAPKs, and the one that phosphorylates mSTAT3 is not clear. However, several MAPKs have been shown to phosphorylate cytosolic STAT3 on the S727 residue, including ERK, p38, PKCδ, and JNK1 (*25*).

Due to its role in mitochondria, STAT3 is especially vital in types of cells with high energy needs, such as osteoblasts and osteoclasts in bone. O_2 consumption is increased when ascorbic acid is added to force cells to differentiate into osteoblasts, and ATP

release is also increased when precursors differentiate into osteoblasts (*24*). This shows that osteoblasts have higher energy needs than the cells from which they are derived.

1.10 Mitochondria

Mitochondria are large organelles that contain two membranes; an outer membrane, which makes up the external surface, and an inner membrane, which is folded into structures called cristae. In between these two membranes is an intermembrane space, and inside the inner membrane is where the mitochondrial matrix is located (*1*).

Mitochondria have their own DNA (mtDNA), separate from the nuclear genome, which is located in the matrix. In most multicellular animals, this DNA is in the form of multiple copies of a circular molecule similar to a bacterial plasmid. MtDNA is cytoplasmically inherited, and is thus 99.99% inherited from the mother (*1*). Although mtDNA is mostly in circular form, it can also be linear in some organisms, and it can also vary greatly in size. MtDNA ranges in size from 6 kb in *Plasmodium* to 2 Mb in melon and cucumber. Mitochondrial genomes can code for anywhere between 7 and 37 genes. These genes are very important to the cell; in fact, large deletions of mitochondrial DNA can cause diseases such as chronic progressive external opthalmoplegia and Kearns-Sayre syndrome, both of which cause eye defects. Vertebrate mitochondrial DNA is 16.5 kb (*26*) and encodes 2 mitochondrial RNAs (12S RNA and 16S RNA), 22 tRNAs used to translate mitochondrial RNAs, and 13 proteins integral to ATP synthesis and the electron transport chain (ND1-ND6, ND4L, Cytochrome b, CO I-III, ATPase 6, and ATPase 8 (*26*)). Another difference between mtDNA and nuclear DNA is in the genetic code. In a

few instances, codons in mitochondrial DNA code for different proteins than in nuclear DNA (*1*).

1.11 Mitochondrial Function

Mitochondria are essential to cellular function due to their production of adenosine triphosphate, or ATP, the energy currency of the cell. The synthesis of ATP is facilitated by redox reactions inside the mitochondria, where electrons are transferred between molecules; one molecule loses electrons (oxidation), and the other molecule gains electrons (reduction). In some cases, hydrogen atoms are transferred at the same time. The energy released in these reactions can be used to produce ATP (*1*).

1.12 Complexes of the ETC

The first complex of the electron transport chain (ETC), also called NADH-CoQ reductase, functions to shuttle two electrons from NADH to CoQ. First, the electrons move from NADH to flavin mononucleotide (FMN), a cofactor related to FAD. FMN is non-covalently bound (*27*), and can accept two electrons, but does so one at a time. The two electrons are then transferred to one of several (*28*) iron-sulfur clusters, then to CoQ. This process oxidizes NADH to NAD^+; the function of Complex I can be investigated by measuring the ratio of NAD^+ to NADH. This process also reduces CoQ to $CoQH_2$. This $CoQH_2$ is then transferred to Complex III. The energy released pumps 4 protons into the intermembrane space, beginning to establish the proton gradient which will later be used for ATP (*1*).

Succinate dehydrogenase, the enzyme that converts succinate to fumarate in the citric acid cycle, also plays a role in electron transport; it is one of the four subunits of complex II of the ETC, succinate-CoQ reductase (*1*). The two electrons released during the conversion of succinate to fumarate are transferred to FAD, which is located in succinate dehydrogenase. The electrons are then transferred through a series of iron-sulfur clusters, which regenerate FAD, and then the electrons are transferred to CoQ that has bound to a cleft in complex II on the matrix side. The $CoQH_2$ formed is then transferred to complex III (*1*).

Complex III functions as a dimer. Complex III accepts two electrons from $CoQH_2$, thus regenerating CoQ, and simultaneously pumps two protons from the matrix into the intermembrane space..The energy of this process is coupled to the pumping of two protons into the intermembrane space and the reduction of a molecule of cytochrome *c*. $CoQH_2$ then dissociates, allowing another molecule of CoQ to bind (*28*).

Complex IV, also called cytochrome *c* oxidase, has the main function of reducing cytochrome *c*. Cytochrome *c* first transfers each electron from its heme group to Cu_a^{2+}, a pair of copper ions in complex IV. The electron then moves to the heme group of cytochrome *a*, then to Cu_b^{2+} and then to the heme in cytochrome a_3; these two structures make up the oxygen reduction center. The electrons are then passed to O_2, the final acceptor, forming water. Four protons are also pumped into the intermembrane space; the mechanism for this process is not known (*1*).

ATP synthase, also called Complex V, functions to manufacture ATP from ADP and P_i, using the protons pumped into the intermembrane space by the first four complexes of the ETC (*1*). It can also hydrolyze ATP to pump protons against an electrochemical gradient (*28*).

1.13 ROS

Reactive Oxygen Species (ROS) are a type of free radical derived from oxygen, and are produced by many bodily functions, including oxidative phosphorylation that occurs in mitochondria (*29*). ROS antagonize Wnt signaling, which is important for osteoblastogenesis, by diverting beta catenin to Forkhead box O mediated transcription (*30*). ROS have also been shown to help induce osteoclast activation, and they are also formed by osteoclasts (*31*). Thus, in several different ways, ROS serve to decrease bone formation and increase bone resorption, increasing the likelihood of osteoporosis. ROS are a type of oxidant; these compounds cause cellular stress when they are in abundance. Antioxidants combat the action of the oxidants (*32*).

1.14 Glutathione and BSO

Glutathione, an antioxidant, fights cellular damage from ROS by serving as an electron donor. This process converts glutathione to glutathione sulfide. As cells age, this process becomes less efficient, and damage from ROS becomes more pronounced (*33*). Buthionine sulfoximine, or BSO, blocks a key step in the synthesis of glutathione, thus decreasing glutathione levels (Slivka, 1988). This is thought to increase ROS levels, and thus, oxidative damage; osteonecrosis has been reported in rats when glutathione depletion was achieved using BSO (*34*).

1.15 Glutathione Synthesis Pathway

γ-glutamylcysteine synthetase is the enzyme that catalyzes the first step in GSH synthesis (*35*). In this step, glutamic acid is bound to cysteine, forming γ-glutamylcysteine. This is the rate-limiting step in GSH synthesis (*36*). In the second step, glycine is added to the compound to form glutathione. BSO is an inhibitor of γ-glutamylcysteine synthetase (*35*) thus blocking the key, rate-limiting step in this reaction.

1.16 Research Goals

We hypothesized that the lack of STAT3 in osteoblasts and osteocytes would cause lower bone formation after mechanical loading. To test this, we deleted exons 18-20 of the STAT3 gene specifically in early murine osteoblasts, and performed mechanical loading. We also hypothesized that STAT3 deficient osteoblasts would produce more ROS than control osteoblasts. We tested this by isolating osteoblasts from both control and KO mice, and assaying for ROS. We also hypothesized that administration of BSO would cause lower bone formation after mechanical loading. We tested this by injecting mice with two doses of BSO, performing mechanical loading, and measuring bone formation parameters.

CHAPTER 2. MATERIALS AND METHODS

2.1 Cre/LoxP Methodology

In conventional knockout mice, the gene of interest is eradicated from the entire organism. Although this method can be useful in some cases, there are others where it is not feasible, such as when the protein made by the gene of interest is vital for survival. Thus, it is very valuable to be able to selectively knock out a gene in just one type of cell. This is also helpful in evaluating the loss of that gene in the specific cell type. The cre/loxP system is a method to accomplish this goal. The recombinase *Cre* is inserted into the genome of a line of mice; this gene is controlled by a cell-specific promoter unique to the type of cell that will be targeted for gene knockout. Another line of mice are created with the gene of interest located between two loxP sites. These loxP sites are recognized by the Cre recombinase when the two lines of mice are bred together, thus excising the gene of interest. The cell-specific promoter ensures that the gene is only knocked out in the desired cell type. Using this system, many different conditional knockouts can be made (*37*). In our case, we used mice with exons 18-20 flanked by two loxP sites (Figure 1). These exons code for the SH2 domain in STAT3, which is the region that is often mutated in diseases of STAT3 deficiency. The cell-specific promoter used was a 3.6 kb fragment of the collagen I promoter; using this promoter serves to target early osteoblasts, which in turn eliminates functional STAT3 in late osteoblasts and

osteocytes as well. After Cre recognizes the loxP sites and excises exons 18-20 of STAT3, exons 17 and 21 are joined with a loxP site in between; exons 18-20 circularize, and contain the other loxP site in between exons 18 and 20. These mice were then denoted Col3.6-Cre;STAT3$^{flox/flox}$ mice, with their control littermates being denoted Col3.6-Cre;STAT3$^{+/+}$ mice.

2.2 Animal Breeding

For the STAT3 study, STAT3 bone specific knockout mice were made using the Cre/LoxP system by breeding Cre recombinase mice (driven by a 3.6 kb fragment of the collagen I promoter) and floxed STAT3 mice. The Cre recombinase transgenic mice were provided by Dr. Barbara Kream of the University of Conneticut Health Center; the floxed STAT3 mice were provided by Dr. Xin-Yuan Fu of the Department of Microbiology and Immunology of the Indiana School of Medicine. Animals homozygous for LoxP STAT3 and had at least one copy of the Cre gene were considered conditional knockouts; animals who were wild type STAT3 and had at least one copy of the Cre gene were considered controls. For the BSO study, C57/BL6 female mice were purchased from Harlan Laboratories and allowed to mature to 16 weeks before injections of BSO were administered. All procedures were performed in accordance with the IUCUC guidelines.

2.3 Genotyping

To perform genotyping, tail snips were obtained from the mice, and the DNA was isolated. The lysis buffer contained 40 mm Tris (pH 8.0), 50 mm KCl, 2.5 mM EDTA, 0.4% NP-40, 0.45% Tween-40. 40 µl of proteinase K (stock 10 mg/ml) was added to the lysis buffer immediately before use; 100 µl of this solution was used per tail snip. This

was incubated overnight in a 56 degree C waterbath. The next morning the samples were incubated in a dry bath for 10 minutes at 95 degrees to inactivate proteinase K, and the lysate was diluted with 100 µl of autoclaved DI water. 1 µl of this solution was then used for PCR. PCR was performed using primers for both Cre and STAT3. The sequences for the Cre primers are as follows: GAGTGATGAGGTTCGCAAGA (Cre-1); CTACACCAGAGACGGAAATC (Cre-2). If positive for Cre, those samples showed a 615 bp size band when run on an agarose gel. If mice were negative for Cre, there was no band, due to Cre not normally being present in mammalian cells. The sequences for the STAT3 primers are as follows: ATTGGAACCTGGGACCAAGTGG (STAT3 Forward); ACATGTACTTACAGGGTGTGTGC (STAT3 Reverse). For STAT3, the WT band was 480 bp, and the floxed band was 520 bp. If an individual mouse was heterozygous, it showed two faint bands very close together. If the genotyping was successful, there were always bands for each sample for STAT3 due to it being constitutively expressed in mammalian cells. Since Cre recombinase was driven by an osteoblast-specific promoter, its expression will be limited to bone tissue, and thus exons 18-20 of STAT3 will only be excised in these specific cells.

2.4 Mechanical Loading

In the STAT3 study, 16 week old mice were subjected to axial loading of the right ulna for 120 cycles at 2 hertz, for three consecutive days, using an electromagnetic actuator (Bose ElectroForce 3200 series; EnduraTEC). The procedure was performed under general anesthesia, using 3-5% isoflurane (Sigma-Aldrich, St. Louis, MO). The peak force used for males was 2.75 N, and for females the peak force used was 2.5 N. The

difference in peak forces for males and females was chosen to ensure that all specimens experienced similar peak strains during loading. The peak strains experienced by wild type mice, both male and female, was approximately 2800 microstrains at the ulna midshaft. For conditional STAT3 knockout mice, the peak strains experienced by both male and female mice ranged between approximately 2940 and 2970 microstrains. The left ulnas were not loaded, and served as internal controls. Calcein was injected 5 days after the first loading bout, and alizarin was injected 9 days after the first loading bout. These injections were administered interperitoneally. Both the right and left ulnas were processed for histomorphometry to evaluate bone formation as a result of mechanical loading; femurs were also collected to determine bone size, bone mineral density and mechanical properties.

In the BSO study, to investigate the role of oxidative stress in bone mechano-responsiveness *in vivo*, we injected female C57BL6 mice with BSO at doses of 800 and 1600 mg/kg 2 hours before we applied mechanical loading using an ulna loading modality with 16-week-old mice using an electromagnetic actuator (Bose ElectroForce 3200 series; EnduraTEC). Subcutaneous injection of BSO to mice leads to a peak tissue level after 2 hrs, coincident with the loading session. BSO blocks a key enzyme in glutathione synthesis and causes a rise in ROS level. The loading conditions were: 120 cycles/day, 3 consecutive days, 2 Hz cycle frequency, with peak forces of 2.6 N. The non-loaded left forearms served as an internal control. The procedure was performed under general anesthesia, using 3-5% isoflurane (Sigma-Aldrich, St. Louis, MO). Calcein was injected 5 days after the first loading bout, and alizarin was injected 9 days after the

first loading bout. These injections were administered interperitoneally. Both the right and left ulnas were processed for histomorphometry to evaluate bone formation as a result of mechanical loading.

2.5 Bone Mineral Content and Bone Mineral Density Measurement

In the STAT3 study, the left femurs were used to measure both bone mineral content (g) and bone mineral density (g/mm^2). This was accomplished using peripheral dual-energy X-ray absorptiometry (pDXA; PIXIMus II; GE-Lunar Co.).

2.6 Biomechanical Testing

In the STAT3 study, femurs were brought to room temperature over a period of approximately two hours in a saline bath, and mechanical testing was conducted by three-point bending using a microforce testing machine (Vitrodyne V1000; Liveco, Inc., Burlington, VT). Loads were applied in the mid-diaphysis region, 10 mm apart from a pair of supports, in the anterposterior direction. Mechanical testing was performed at a cross-head speed of 0.2 mm/s. We measured ultimate force (N), stiffness (N/mm), and work to failure (mJ).

2.7 Histomorphometry

Bone specimens were immersed in 10% neutral buffered formalin for 48 hours, then dehydrated in graded alcohols, cleared in xylene, then embedded in methyl methacrylate (MMA). Transverse thick sections (70 μm) were cut using a diamond-embedded wire saw (Histo-saw; Delaware Diamond Knives, Wilmington, DE). These sections were then

ground down to approximately 20 μm and mounted on microscope slides. Three sections per limb were used for histomorphometry with a Nikon Optishot fluorescence microscope (Nikon, Inc., Garden City, NJ) using a Bioquant digitizing system (R&M Biometrics, Nashville, TN). The following primary data was collected from the periosteal surface at 250x magnification: total perimeter (B.Pm); single label perimeter (sL.Pm); double label perimeter (dL.Pm), and double label area (dL.Ar). From this primary data, the following quantities were derived: (mineralizing surface (MS/BS=[1/2sL.Pm + dL.Pm]/B/Pm x 100; %); mineral appositional rate (MAR=dL.Ar/dL.Pm/6days; μm/day) and bone formation rate (BFR/BS=MAR x MS/BS x 3.65; $\mu m^3/\mu m^2$/year). A set of relative values (rMS/BS, rMAR, and rBFR/BS) was obtained in which the nonloaded, internal control for each experiment was subtracted from the loaded ulna, thus eliminating any bone formation that occurred in that particular animal independent of mechanical loading.

In the STAT3 study, the femurs were cut into 5μm thick frontal sections using a microtome (Leica, Germany). Two unstained sections were mounted onto microscope slides, and other sections were stained with McNeal's tetrachrome, as well as tartrate-resistant acid phosphatase (TRAP) to identify active osteoclasts. The following data was collected from the metaphyseal area at 250x magnification: tissue area (T.Ar), trabecular bone area (tB.Ar), trabecular bone perimeter (tB.Pm), single label perimeter (sL.Pm), double label perimeter (dL.Pm), double label area dL.Ar), osteoclast surface (Oc.S), and osteoclast number (Oc.N). From this primary data, the following quantities were derived: bone volume (BV/TV=tB.Ar x 100; %), mineralizing surface

(MS/BS=[1/2sL.Pm+dL.Pm]/B.Pm x 100; %), mineral appositional rate (MAR=dL.Ar/dL.Pm/6 days; μm/day), bone formation rate (BFR/BS=MAR x MS/BS x 3.65; $\mu m^3/\mu m^2$/year), percentage of osteoclast surface (Oc.S/BS=Oc.S/tB.Pm; %), and osteoclast number per mm (Oc.N/Bs=Oc.N/tB.Pm; #/mm).

2.8 Cell Culture

The pre-osteoblastic cell murine cell line, MC3T3-E1, was cultured in α-MEM (Sigma, St. Louis, MO, USA) containing 10% FBS (Atlanta Biologicals, Norcross, GA), 100 U/ml penicillin G (Sigma), and 100 μg/ml streptomycin (Sigma). These cells were maintained in a humidified incubator containing 95% air and 5% CO_2, kept at 37 degrees Celsius, and subcultured approximately every 72 hours. Primary osteoblasts were isolated from calvarial bone of 4.5-day-old STAT3 deficient mice (Col3.6-Cre;$STAT3^{flox/flox}$) and littermate controls (Col3.6-Cre;$STAT3^{+/+}$) by sequential digestions with collagenase and trypsin. We added 50 μg/ml ascorbic acid and cultured for 21 days to induce osteoblast differentiation. Then the cells were used for the measurement of ROS and NAD^+/NADH ratio.

2.9 FSS Studies

For fluid shear experiments, MC3T3-E1 cells or primary osteoblasts were plated on type I collagen-coated (10 $\mu g/cm^2$, BD Biosciences, Bedford, MA) 75x38 mm^2 glass slides (Fisher Scientific, Pittsburgh, PA) at a density of about 1 x 10^5 cells/cm^2. The cells were serum-starved for 24 h in α-MEM supplemented with 0.2%FBS prior to flow. Cells were subjected to oscillatory fluid shear stress (12 dynes/cm^2) in parallel plate flow chambers

at 37°C using a previously described fluid flow device (*38*). Hard walled tubing was used to connect the pump to the chamber inlet, and a reservoir was attached to the outlet to allow for movement of the fluid and exchange of 5% CO_2. This system subjected cells to oscillating fluid flow at a frequency of 1 Hz in α-MEM supplemented with 0.2%FBS and antibiotics. Static controls were held in cell culture dishes at 37°C with 5% CO_2.

2.10 Western Blot Analysis

Immediately after MC3T3-E1 cells were subjected to FSS for 30, 60 and 90 minutes, the cells were washed quickly with cold PBS (1x) and lysed with SDS lysis buffer. The lysis buffer contained 62.5mM Tris, 2% sodium dodecyl sulfate (SDS), 10% glycerol (v/v), 5 mM EDTA, and 1% protease inhibitor cocktail (Sigma). After the cell lysates were boiled for 10 min, the protein samples were centrifuged at 14,000 g for 10 min at 4°C to remove any cellular debris. Protein assay was performed using a Bio-Rad detergent compatible (DC) protein assay. Twenty micrograms of whole cell lysates were separated by 10% SDS-polyacrylamide gel electrophoresis and electrotransferred to a nitrocellulose membrane. Membranes were blocked in Tris-buffered saline containing 5% nonfat dry milk and 0.1% Tween-20 (TBST), and incubated with 200 μg/ml (1:1000) rabbit anti-STAT3 and rabbit anti-p-STAT3 (Ser 727) antibodies (Santa Cruz Biotechnology, Santa Cruz, CA) overnight at 4°C. Following three washes in TBST, the membranes were incubated with goat anti-rabbit IgG hydroperoxidase conjugated secondary antibodies (1:5000) for 1 h at room temperature. Immunodetection was conducted using the enhanced chemiluminescence (ECL) method.

2.11 Measurement of ROS

To measure ROS in the STAT3 study, the cell-permeable dye 2,7-dichlorodihydrofluorescein diacetate (2,7-DCF-DA) (Sigma-Aldrich), was used. Cells from both wild type and knockout calvarias were plated in 6 well plates in full serum media for 24 hours. Cells were then treated with μM H_2O_2 as a positive control (to stimulate ROS production). This was done both in the presence and absence of 50 μM Ag-490, a STAT3 inhibitor, for 2 hours. Cells were then suspended with 10 μM 2,7-DCF-DA, and assayed for ROS using flow cytometry.

2.12 Statistical Analysis

The data are expressed as mean ± SEM (standard error of the mean). Phenotypic values among the selected genotypes for a given sex were compared by one-way analysis of variance (ANOVA). Gender comparisons were performed using a two-way ANOVA with sex and genotype as independent variables. Differences between the loaded (right) and nonloaded (left) limbs were tested using paired t-tests. Statistical significance was assumed for $p<0.05$.

CHAPTER 3. RESULTS

A deletion of the exons 18 through 20 resulted in a conditional knockout of STAT3 protein in the osteoblasts and osteocytes (Figure 1), which was confirmed by immunohistochemical staining. Note that about 10% of the STAT3 deficient mice were extremely small and exhibited a spine deformity, which was noticeable at age of 3-4 weeks (Figure 2). Those mice were unable to survive longer than 8 weeks and were excluded in the current study.

The bone phenotypes were characterized when they were 18 weeks old. Female Col3.6-Cre;STAT3 $^{flox/flox}$ mice had significantly smaller body weights (-11%, $p=0.02$) compared with Col3.6-Cre;STAT3 $^{+/+}$ mice, whereas the average body mass was not statistically different in male KO and littermate mice (Figure 3). Femur length was significantly shorter in the mutants for both male and female mice (Figure 4). The conditional STAT3 KO mice exhibited low bone mass phenotype, and BMC (-13% in female, $p<0.01$ and -11% in male, $p<0.05$; (Figure 5) and BMD (-7% in female, $p<0.05$ and -12% in male, $p<0.001$) were significantly lower in KO than control littermates (Figure 6).

Bone histomorphometry was conducted using trabecular bones at distal femurs. For both female and male mice, bone volume was significantly less in KO (Col3.6-Cre;STAT3 $^{flox/flox}$) mice (-39% in female, $p<0.05$ and -38% in male, $p<0.05$; Figure 7) than their littermate controls. Furthermore, mineralizing surface (MS/BS, -24% in female, $p<0.05$ and -29% in male, $p<0.05$; Figure 8), mineral appositional rate (MAR, -54% in female, $p<0.002$ and -56% in male, $p<0.05$, Figure 9) and bone formation rate (BFR/BS, -63% in female, $p<0.001$ and -65% in male, $p<0.05$; Figure 10) were significantly smaller in KO mice than control mice. Although the number of osteoclasts was statistically similar between KO mice and their control mice, osteoclast surfaces were significantly greater in KO mice (+39% in female and +40% in male, $p<0.05$; Figure 11) than their littermates.
In order to evaluate the mechanical properties of bone in KO (Col3.6-Cre;STAT3 $^{flox/flox}$) mice and control mice, the femurs were subject to mechanical testing. For both sexes, the ultimate forces (-28% in female, $p<0.01$ and -27% in male, $p<0.01$; Figure 12) and stiffness (-36% in female, $p<0.01$ and -40% in male, $p<0.001$; Figure 13) were reduced significantly in KO mice in comparison with their controls. This data suggests that inactivation of STAT3 specific to osteoblasts and osteocytes significantly decreases bone strength. Work to failure in the female mutant mice was statistically lower than in control females ($p<0.05$), while the male work to failure difference was not statistically significant (Figure 14).

To investigate the role of STAT3 in load-driven bone formation, the Col3.6-Cre;STAT3 $^{flox/flox}$ mice as well as their littermate control mice (Col3.6-Cre;STAT3 $^{+/+}$) were given ulna loading and their bone formation responses were evaluated. The results showed that

load-induced bone formation was suppressed in male and female Col3.6-Cre;STAT3 $^{flox/flox}$ mice. The data from female Col3.6-Cre;STAT3 $^{flox/flox}$ mice is shown in Figures 15 and 16. In female mice, for instance, the relative bone formation rate (BFR/BS in the right ulna minus BFR/BS in the left ulna) was roughly 56% lower in Col3.6-Cre;STAT3 $^{flox/flox}$ mice. This loading data support an important role of STAT3 in load-driven bone formation.

To demonstrate the STAT3 activation in response to FSS, we examined the phosphorylation of STAT3 at serine 727 using MC3T3-E1 osteoblastic cells in the presence and absence of FSS (12 dyn/cm^2). Western blotting analysis showed that serine phosphorylation of STAT3 increased in a manner dependent on flow duration from 30 to 90 min (Figure 17).

In order to examine if STAT3 deficiency led to an elevated level of intracellular ROS, calvarial osteoblasts were cultured and assayed for ROS using DCF-DA and flow cytometry. The ROS level was significantly higher in STAT3 deficient osteoblasts than control cells (Figure 18). Furthermore, administration of STAT3 inhibitor, AG490, significantly increased the production of ROS in control cells, but it did not affect the ROS level in STAT3 deficient osteoblasts. This data suggests that the inactivation of STAT3 both in KO osteoblasts as well as in AG-490 treated control osteoblasts increases the intracellular ROS level.

To investigate the role of oxidative stress in bone mechano-responsiveness *in vivo*, we injected female C57BL6 mice with BSO at doses of 800 and 1600 mg/kg 2 hours before we applied mechanical loading using an ulna loading modality with 16-week-old mice. Histomorphometric data demonstrated that load-induced bone formation, including relative label surface (rLS/BS), relative mineral appositional rate (rMAR) and relative bone formation rate (rBFR/BS), was dramatically suppressed in the mice pre-treated with both low (800 mg/kg) and high (1600 mg/kg) doses of BSO compared to the control treated with phosphate buffered saline (PBS) (Figures 20 & 21, a: $p<0.05$; b: $p<0.01$; c: $p<0.001$ versus PBS). These data suggest that mitochondrial activity plays an important role in mechanical stimulation.

CHAPTER 4. DISCUSSION

The present study demonstrated that inactivation of STAT3 in osteoblasts and osteocytes reduced bone mass, strength, and load-driven bone formation. Furthermore, STAT3 deficient osteoblasts presented a higher basal level of ROS, and mechanical stimulation failed to lower this ROS level. These results clearly show that STAT3 plays a critical role in bone homeostasis and mechanotransduction, and STAT3 is involved not only in load-driven gene activation in nucleus but also in regulation of ROS and oxidative stress in mitochondria.

Consisent with a previous study (*39*) our study has shown that osteoblast/osteocyte specific knockout of STAT3 results in an osteoporotic phenotype because of suppressed bone formation. We have shown that STAT3 deficiency in osteoblasts/osteocytes does not change the number of osteoclasts, but osteoclast surfaces were significantly greater in KO mice than their littermates. Since osteoclast surface is normalized by bone surface, there is a possibility that the greater osteoclast surfaces in STAT3 deficient mice may result from the reduced bone surfaces due to the inhibition of bone formation. In addition, our study has demonstrated that STAT3 deficiency in osteoblasts/osteocytes leads to a reduction in mechanical properties of mouse long bones.

This data suggests that STAT3 plays an important role in bone homeostasis and maintenance of bone strength.

The difference in femur length between STAT3 knockouts and wildtype controls raises the question: which is responsible, bone modeling, or bone remodeling? To determine this, an experiment could be designed where earlier bone formation (i.e. bone modeling) would be differentiated from later bone formation (i.e. bone remodeling). This could be achieved by determining the time point where bone modeling is replaced by bone remodeling, and measuring the difference in femur length at both of these time points in conditional STAT3 knockout mice versus wildtype controls. The fact that body mass was affected in female conditional knockouts, and not males, suggests that estrogen and/or progesterone may be implicated in the role of STAT3 in load-induced bone formation.

Mechanically induced bone formation was suppressed in both male and female conditional STAT3 KO mice. Because of the reduced mineralizing surface and mineral appositional rate, the result indicates that STAT3 deficiency suppresses osteoblast recruitment and activity. The mechanism of STAT3 activation is considered to be linked to the gp130 signaling pathway. Targeted disruption of the gp130 gene in mice leads to embryonic lethality (*40*). The gp130 knockout mice demonstrate defects in bone development, formation and resorption (*5*,*41*). Osteoblastic cells express a group of receptors for cytokines such as IL6 and IL11, which share the gp130 signal transducer (*42*). IL6, for instance, has been shown to be elevated in calvarial osteoblasts in response to mechanical stimulation (*43*), and IL11 is also increased in response to loading *in vivo*

as well as FSS *in vitro* (*44*). Furthermore, anti-IL11 antibody is shown to black mechanically induced enhancement of bone formation. Thus, is it possible that in STAT3 KO mice gp130 signaling is blocked, impairing proliferation and differentiation of osteoblasts.

As a downstream mechanism for STAT3-mediated bone formation, STAT3 regulates functions in both nuclei and mitochondria. STAT3 is activated by tyrosine phosphorylation, which dimerizes and translocates it to the nucleus (*14*). It binds specific gene-promoter sequences and induces gene expression (*14*,*45*-*6*). Furthermore, STAT3 regulates cell respiration and metabolism in mitochondria (*19*,*24*). Without STAT3, an electron transport chain (ETC) is inhibited and reduction in mitochondrial activity leads to accumulation of ROS (*45*-*7*). Therefore, inhibition of bone formation in the conditional STAT3 KO mice may result from the suppression of gene expression and elevation of ROS in osteoblasts.

Regarding gene regulation in nucleus, disruption of STAT3 likely alters expression of mechanosensitive genes such as Wnt molecules. In stromal cells transforming growth factor (TGF)-β mediated inhibition of Wnt3a is in part through the suppression of STAT3 (*48*).

Our unpublished data as indicate that STAT3 regulates expression of Wnt5a in osteoblasts. Both Wnt3a and Wnt5a have previously shown to stimulation osteoblast proliferation and differentiation (*49*-*50*). Using the conditional STAT3 deficient mice in

this study, our future study may include identification of load-drive up-stream genes in the presence and absence of STAT3 in osteoblasts.

It has been known that accumulation of ROS is associated with osteoporosis and aging related bone loss. Recently, STAT3 has been shown to connect mitochondrial functions to ROS production in hepatocytes and cardiomyocytes (*24*). In order to investigate whether STAT3 inactivation would regulate the ROS level and mitochondrial functions in osteoblasts, we applied FSS on STAT3 deficient calvarial osteoblasts. First, we showed that serine phosphorylation of STAT3 increased from 30 to 90 min following FSS, suggesting the sustained STAT3 activation in response to mechanical stimulation. Especially, the conserved serine phosphorylation site on STAT3 is critical in regulation of mitochondrial activities (*24*). Next, we demonstrated STAT3-driven association of the level of ROS through mitochondrial activity with the effects of mechanical loading on bone formation. The result presented a significant increase in ROS in STAT3 deficient osteoblasts. Furthermore, FSS reduced the level of ROS through stimulation of mitochondrial activity but it failed to do so in STAT3 deficient osteoblasts. Clinical evidence suggests that age related bone loss is closely associated with oxidative stress (*51-4*). In addition, recent studies have demonstrated that oxidative stress antagonizes Wnt signaling (*3,55*). It has yet to be tested whether reduction in load-driven bone formation in STAT3 KO mice is in part caused by an increase in the basal level of ROS and/or insensitivity of ROS levels in response to mechanical loading.

In order to further investigate the role of oxidative stress in bone mechano-responsiveness *in vivo*, we injected female C57BL6 mice with BSO at doses of 800 and 1600 mg/kg 2 hours before we applied mechanical loading using an ulna loading modality with 16-week-old mice. The histomorphometric data demonstrated that load-induced bone formation, including relative label surface (rLS/BS), relative mineral appositional rate (rMAR) and relative bone formation rate (rBFR/BS), was dramatically suppressed in the mice pre-treated with both low (800mg/kg) and high (1600 mg/kg) doses of BSO compared to the control treated with phosphate buffered saline (PBS). This data suggests that mitochondrial activity plays an important role in mechanical stimulation *in vivo*.

In the current study, both osteoblasts and osteocytes are deficient in STAT3. It has been proposed that osteocytes are mechanosensing cells in bone. Thus, there is a possibility that suppression of load-driven bone formation in this study is primarily caused by STAT3 deficiency in osteocytes. Future studies using osteocyte specific inactivation of STAT3 might further differentiate the role of STAT3 in osteoblasts and osteocytes.

In conclusion, loss-of-function mutations of STAT3 reduce bone mass and load-driven anabolic responses, and STAT3 plays a critical role in regulation of anabolic pathways in the nucleus as well as suppression of ROS in mitochondria.

LIST OF REFERENCES

LIST OF REFERENCES

1. H. Lodish, *et al., Molecular Cell Biology* (W.H. Freeman and Co., ed. 6, 2008).
2. G. Karsenty, E.F. Wagner, Reaching a genetic and molecular understanding of skeletal development. *Dev Cell* **2**(4):389-406 (April 2002).
3. T.J. Chambers, Regulation of the differentiation and function of osteoclasts. *J Pathol* **192**(1):4-13 (September 2000).
4. O. Kudo, Interleukin-6 and Interleukin-11 support human osteoclast formation by a RANKL-independent mechanism. *Bone* **32**(1):1-7 (January 2003).
5. H.I. Shin, *et al.,* Gp-130 mediated signaling is necessary for normal osteoblastic function *in vivo* and *in vivo*. *Endocrinology* **145**(3):1376-85 (March 2004).
6. M. Karst, G. Gorny, R.J. Galvin, M.J. Oursler, Roles of stromal cell RANKL, OPG, and M-CSF expression in biphasic TGF-beta regulation of osteoclast differentiation. *J Cell Physiol* **200**(1):99-106 (July 2004).
7. S. Srinivasan *et al.,* Role of mitochondrial reactive oxygen species in osteoclast differentiation. *Ann N Y Acad Sci* **1192**:245-52 (March 2010).
8. S.R. Young, J.M. Hum, E. Rodenberg, C.H. Turner, F.M. Pavalko, Non-overlapping functions for Pyk2 and FAK in osteoblasts during fluid shear stress-induced mechanotransduction. *PloS One* **6**(1):e16026 (January 2011).

9. L. Liu, W. Yuan, J. Wang, Mechanisms for osteogenic differentiation of human mesenchymal stem cells induced by fluid shear stress. *Biomech Model Mechanobiol* 9(6):659-70 (December 2010).
10. B. Rath, *et al.,* Biomedical forces exert anabolic effects on osteoblasts by activation of SMAD 1/5/8 through type 1 BMP Receptor. *Biorheology* **48**(1):37-48 (2011).
11. H. Zhou, *et al.,* Osteoblast/osteocyte-specific inactivation of STAT3 decreases load-driven bone formation and accumulates reactive oxygen species. *Bone* **49**(3):404-11 (September 2011).
12. J.C. Gallagher, A.J. Sai, Molecular biology of bone remodeling: implications for new therapeutic targets for osteoporosis. *Maturitas* **65**(4):301-7 (April 2010).
13. Z. Stark, R. Savarirayan, Osteopetrosis. *Orphanet J Rare Dis* **4**:5 (February 2009).
14. J.E. Darnell, STATs and gene regulation. *Science* **277**(5332):1630-5 (September 1997).
15. K. Takeda, *et al.,* Targeted disruption of the mouse STAT3 gene leads to early embryonic lethality. *Proc Natl Acad Sci U S A* **94**(8):3801-4 (April 15, 1997).
16. T. Matsuda, *et al.,* STAT3 activation is sufficient to maintain an undifferentiated state of mouse embryonic stem cells. *EMBO J* **18**(15):4261-9 (August 1999).
17. T. Welte, STAT3 deletion during hematopoiesis causes Crohn's disease-like pathogenesis and lethality: a critical role of STAT3 in innate immunity. *Proc Natl Acad Sci U S A* **100**(4):1879-84 (February 2003).

18. Z. Guo, H. Jiang, X. Xu, W. Duan, M.P. Mattson, Leptin-mediated cell survival signaling in hippocampal neurons mediated by JAK STAT3 and mitochondrial stabilization. *J Biol Chem* **283**(3):1754-63 (January 2008).
19. C. Lufei, *et al.*, GRIM-19, a death-regulatory gene product, suppresses STAT3 activity via functional interaction. *EMBO J* **22**(6):1325-35 (March 2003).
20. D.S. Aaronson, C.M. Horvath, A road map for those who don't know JAK-STAT. *Science* **296**(5573):1653-5 (May 31, 2002).
21. I.M. Fearnley, *et al.*, GRIM-19, a cell death regulatory gene product, is a subunit of bovine mitochondrial NADH:ubiquinone oxidoreductase (complex I). *J Biol Chem* **276**(42):38345-8 (October 2001).
22. U.A. White, J.M. Stephens, The gp130 receptor cytokine family: regulators of adipocyte development and function. *Curr Pharm Des* **17**(4):340-6 (2011).
23. S.M. Holland, *et al.*, STAT3 mutations in the hyper-IgE syndrome. *N Engl J Med* **357**(16):1608-19 (October 2007).
24. J.R. Wegrzyn, *et al.*, Function of mitochondrial STAT3 in cellular respiration. *Science* **323**(5915):793-7 (February 2009).
25. T. Decker, P. Kovarik, Serine phosphorylation of STATs. *Oncogene* **19**(21):2628-37 (May 2000).
26. P.F. Chinnery, Mitochondrial disorders overview. In *GeneReviews[Internet]*, R.A. Pagon, T.D. Bird, C.R. Dolan, K Stephens, M.P. Adam, editors. Seattle (WA): University of Washington, Seattle; 1993-2000 June 08 [updated 2010 .September 16].

27. I.M. Fearnley, J. Carroll, J.E. Walker, Proteomic analysis of the subunit composition of Complex I (NADH:ubiquinone oxidoreductase) from bovine heart mitochondria. *Methods Mol Biol* **357**:103-25 (2007).
28. M. Saraste, Oxidative phosphorylation at the fin de siècle. *Science* **283**(5407):1488-93 (March 1999).
29. T.P. Devasagayam, *et al.,* Free radicals and antioxidants in human health: current status and future prospects. *J Assoc Physicians India* **52**:794-804 (October 2004).
30. M. Almeida, L. Han, M. Martin-Millan, C.A. O'Brien, S.C. Manolagas, Oxidative stress antagonizes Wnt signaling in osteoblast precursors by diverting beta-catenin from T cell factor to forkhead box O-mediated transcription. *J Biol Chem* **282**(37):27298-305 (September 2007).
31. H. Ha, Reactive oxygen species mediate RANK signaling in osteoclasts. *Exp Cell Res* **301**(2):119-27 (December 2004).
32. H. Sies, Oxidative stress: oxidants and antioxidants. *Exp. Physiol* **82**(2):291-5 (March 1997).
33. I. Rebrin, R.S. Sohal, Pro-oxidant shift in glutathione redox state during aging. *Adv Drug Deliv Rev* **60**(13-14):1545-52 (October-November 2008).
34. T. Ischiseki, *et. al.,* Oxidative stress by glutathione depletion induces osteonecrosis in rats. *Rheumatology* **45**(3):287-90 (March 2006).
35. A. Slivka, M.B. Spina, H.I. Calvin, G. Cohen, Depletion of brain glutathione in preweanling mice by L-buthionine sulfoximine. *J Neurochem* **50**(5):1391-3 (May 1988).

36. C.C. White, H. Viernes, C.M. Krejsa, D. Botta, T.J. Kavanagh, Fluorescence-based microtiter plate assay for glutamate-cysteine ligase activity. *Anal Biochem.* **318**(2):175-80 (July 2003).

37. S.A. Heldt, K.J. Ressler, The use of lentiviral vectors and Cre/loxP to investigate the function of genes in complex behaviors. *Front Mol Neurosci* **2**:22 (2009).

38. C.R. Jacobs, *et al.,* Differential effect of steady versus oscillating flow on bone cells. *J Biomech* **31**(11):969-76 (November 1998).

39. S. Itoh *et al.,* A critical role for interleukin-6 family-mediated Stat3 activation in osteoblast differentiation and bone formation *Bone* **39**(3):505-12 (September 2006).

40. K. Yoshida, *et al.,* Targeted disruption of gp130, a common signal transducer for the interleukin 6 family of cytokines, leads to myocardial and hematological disorders. *Proc Natl Acad Sci U S A* **93**(1):407-11 (January 1996).

41. K. Kawasaki, *et al.,* Osteoclasts are present in gp130-deficient mice. *Endocrinology* **138**(11):4959-65 (November 1997).

42. T. Bellido, *et al.,* Detection of receptors for interleukin-6, interleukin-11, leukemia inhibitory factor, oncostatin M, and ciliary neurotrophic factor in bone marrow stromal/osteoblastic cells. *J Clin Invest* **97**(2):431-7 (January 1996).

43. C. Sanchez, O. Gabay, C. Salvat, Y.E. Henrotin, F. Berenbaum, Mechanical loading highly increases IL-6 production and decreases OPG expression by osteoblasts. *Osteoarthritis Cartilage* **17**(4):473-81 (April 2009).

44. S. Kido, *et al.,* Mechanical stress induces interleukin-11 expression to stimulate osteoblast differentiation. *Bone* **45**(6):1125-32 (December 2009).

45. N.C. Reich, L. Liu, Tracking STAT nuclear traffic. *Nat Rev Immunol* **6**(8):602-12 (August 2006).

46. M.G. Myers, Moonlighting in mitochondria. *Science* **323**(5915):723-4 (February 2009).

47. G. Hajnoczky, J.B. Hoek, Mitochondrial longevity pathways. *Science* **315**(5812):607-9 (February 2007).

48. X. Li, *et al.*, Prostate tumor progression is mediated by a paracrine TGF-beta/Wnt3a signaling axis. *Oncogene* **27**(56):7118-30 (November 2008).

49. H. Zhou, W. Mak, Y. Zheng, C.R. Dunstan, M.J. Seibel, Osteoblasts directly control lineage commitment of mesenchymal progenitor cells through Wnt signaling. *J Biol Chem* **283**(4):1936-45 (January 2008).

50. M. Katoh, Transcriptional mechanisms of Wnt5a based on NF-kappaB, Hedgehog, TGFbeta, and Notch signaling cascades. *Int J Mol Med* **23**(6):763-9 (June 2009).

51. X.C. Bai, *et al.*, Oxidative stress inhibits osteoblastic differentiation of bone cells by ERK and NF-kappaB. *Biochem Biophys Res Commun* **314**(1):197-207 (January 2004).

52. S. Basu, K. Michaelsson, H. Olafsson, S. Johansson, H. Melhus, Association between oxidative stress and bone mineral density. *Biochem Biophys Res Commun* **288**(1):275-9 (October 2001).

53. G. Kasper, *et al.*, Insights into mesenchymal stem cell aging; involvement of antioxidant defense and actin cytoskeleton. *Stem Cells* **27**(6):1288-97 (June 2009).

54. S.S. Varanasi, R.M. Francis, C.E. Berger, S.S. Papiha, H.K. Datta, Mitochondrial DNA deletion associated oxidative stress and severe male osteoporosis, *Osteoporosis Int* **10**(2):143-9 (1999).

55. M. Almeida, E. Ambrogini, L. Han, S.C. Manolagas, R.L. Jilka, Increased lipid oxidation increases oxidative stress, increased peroxisome proliferator-activated receptor-gamma expression, and diminished pro-osteogenic Wnt signaling in the skeleton. *J Biol Chem* **284**(40):27438-48 (October 2009).

FIGURES

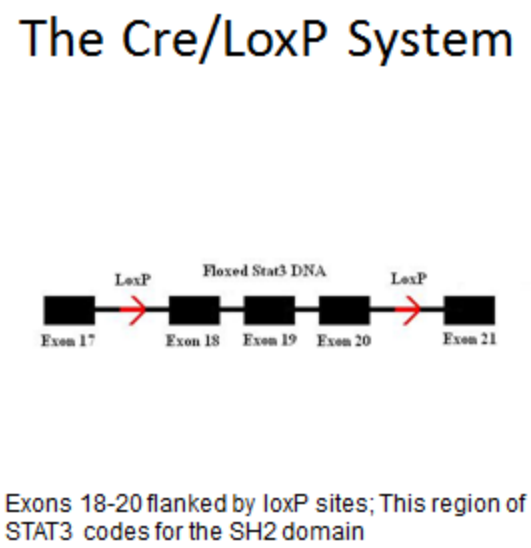

Figure 1: Floxed STAT3 DNA.

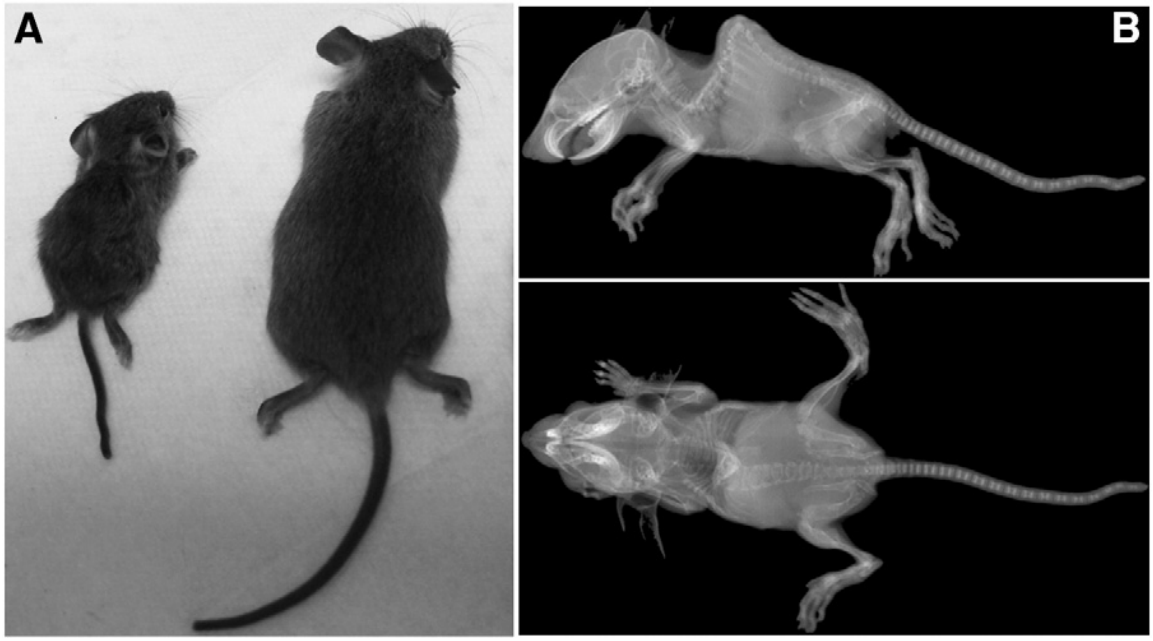

Figure 2: Appearance of the conditional STAT3 KO mice.

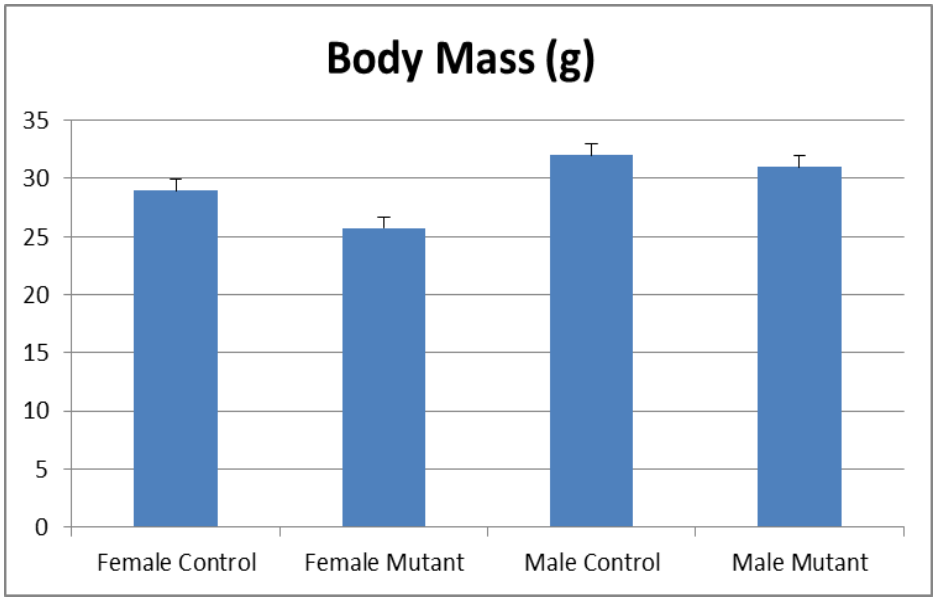

Figure 3: Body mass comparison.

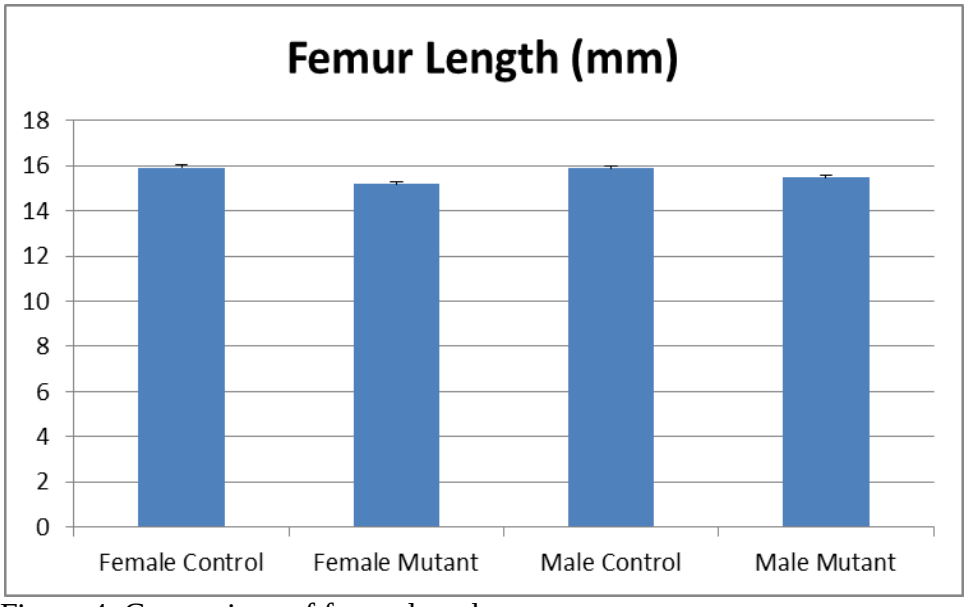

Figure 4: Comparison of femur length.

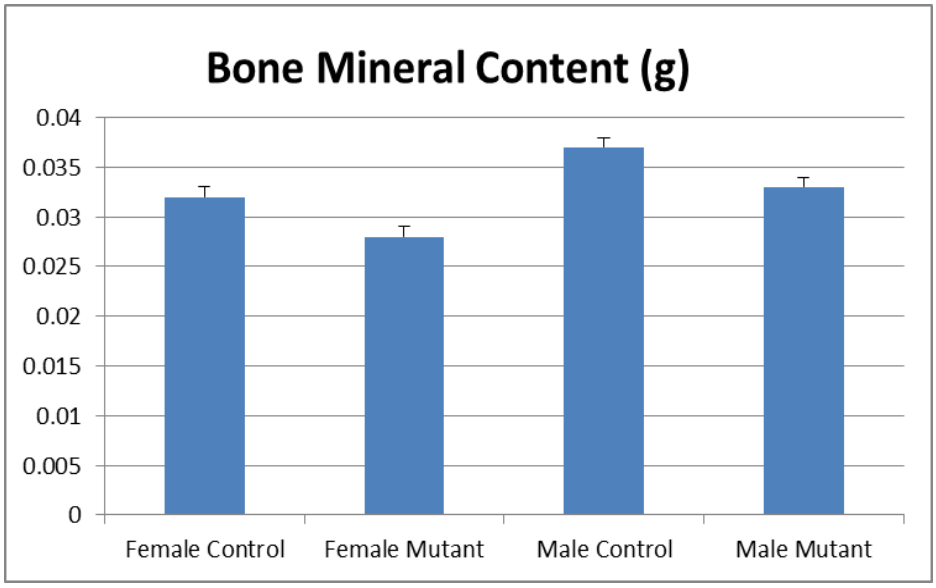

Figure 5: Comparison of bone mineral content.

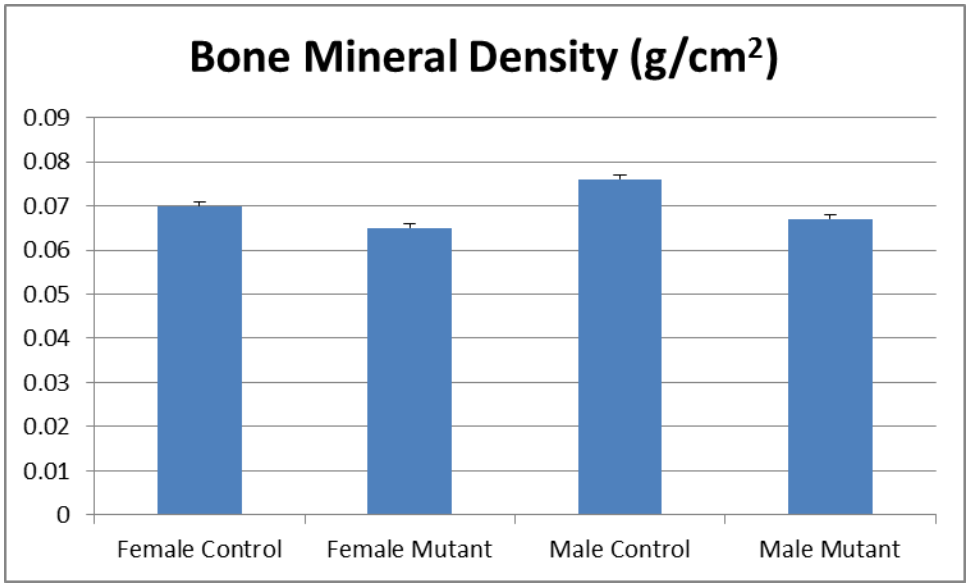

Figure 6: Comparison of bone mineral density.

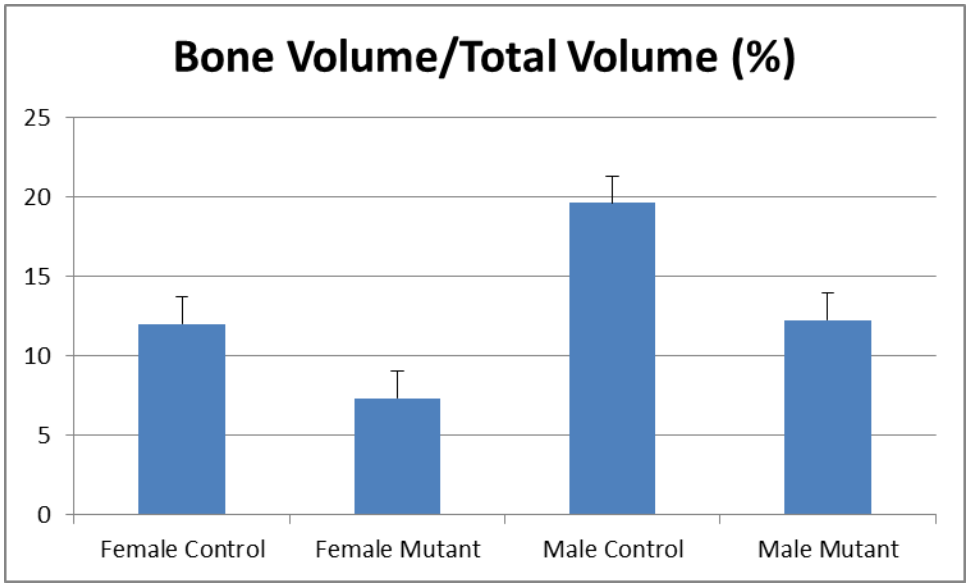

Figure 7: Comparison of bone volume.

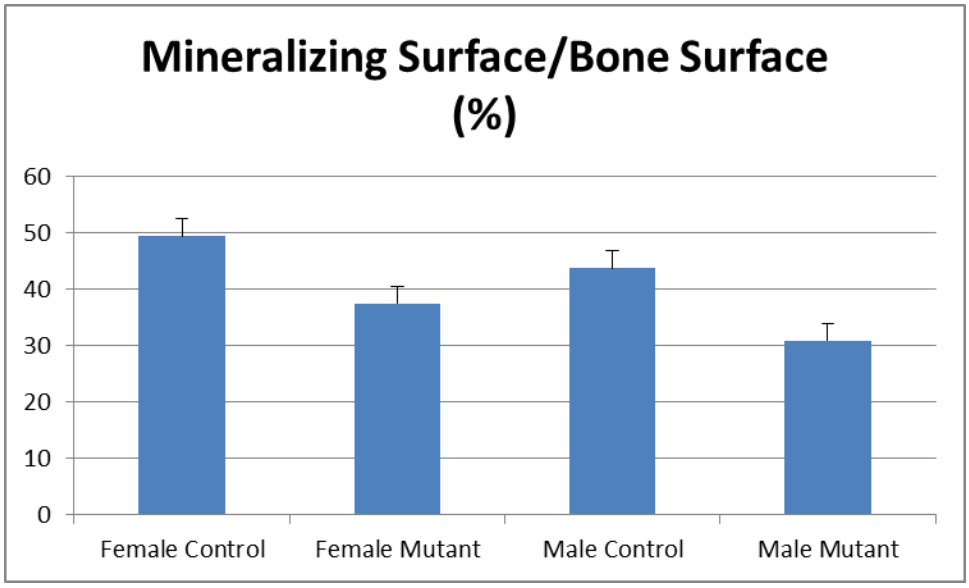

Figure 8: Comparison of mineralizing surface.

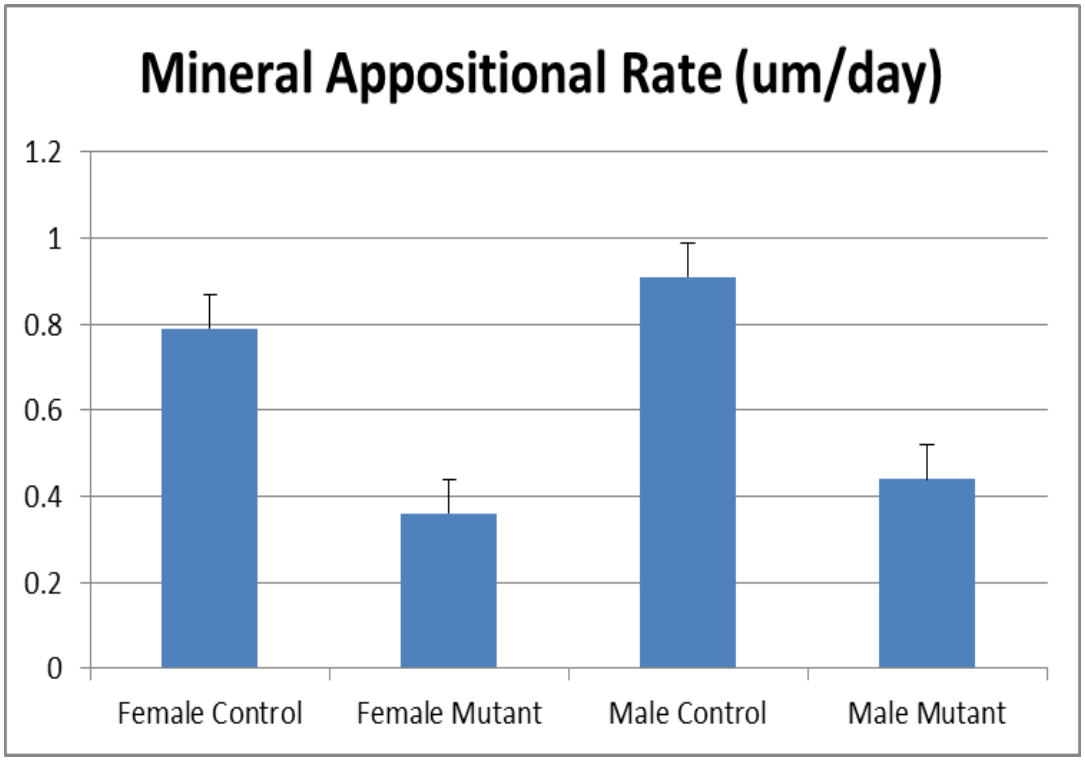

Figure 9: Comparison of mineral appositional rate.

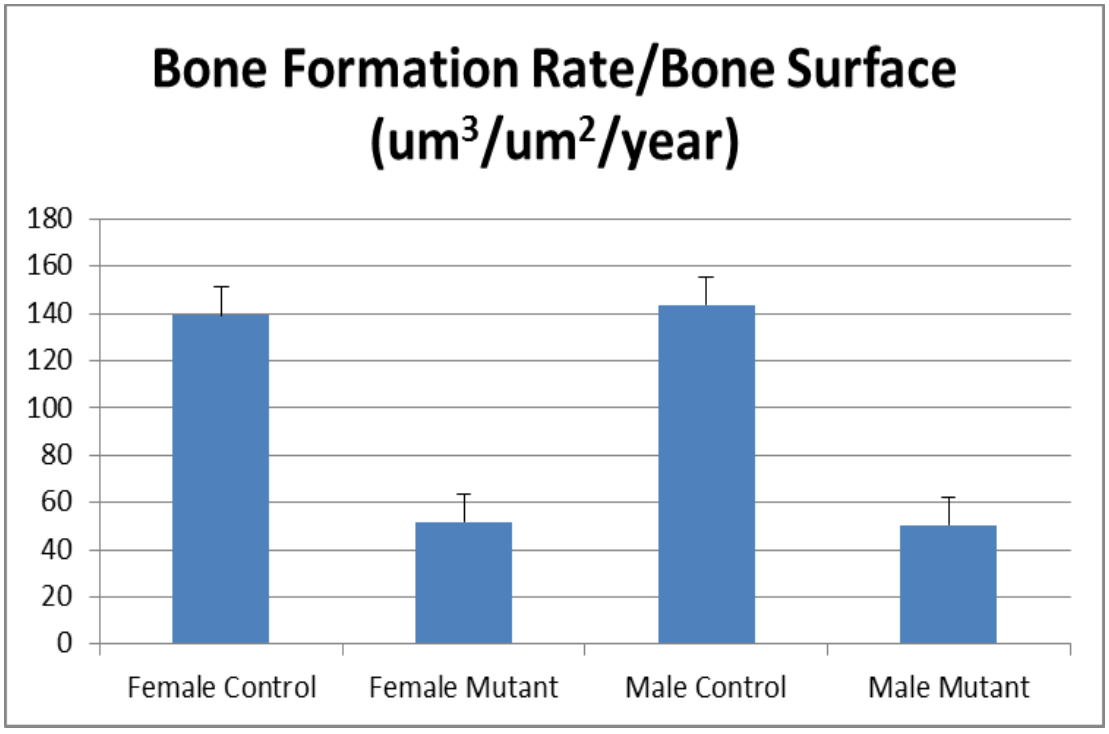

Figure 10: Comparison of bone formation rate.

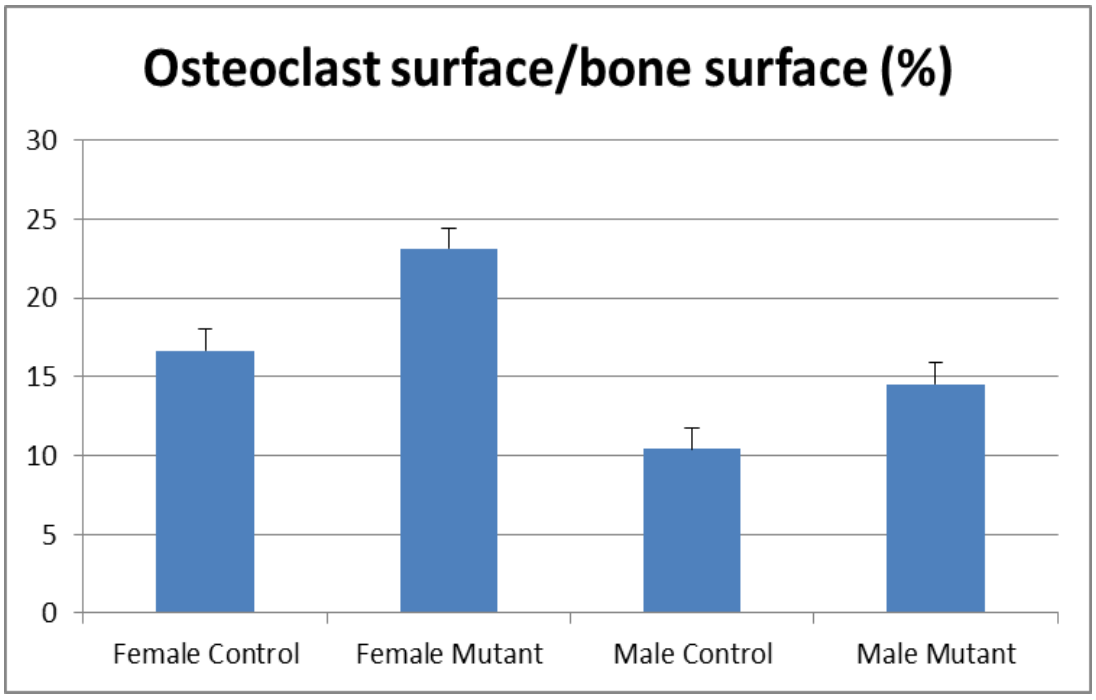

Figure 11: Comparison of osteoclast surface.

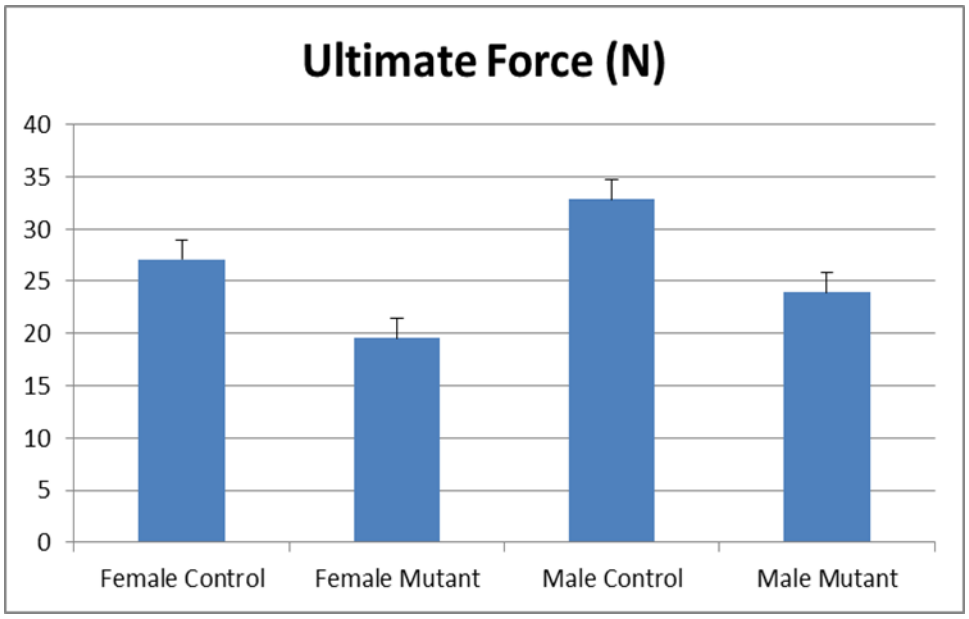

Figure 12: Comparison of ultimate force.

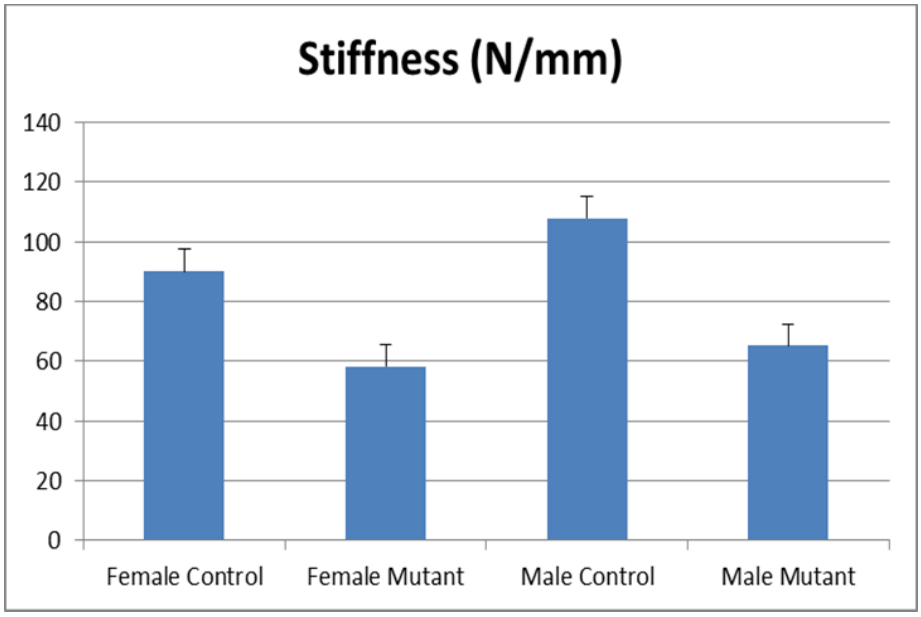

Figure 13: Comparison of stiffness.

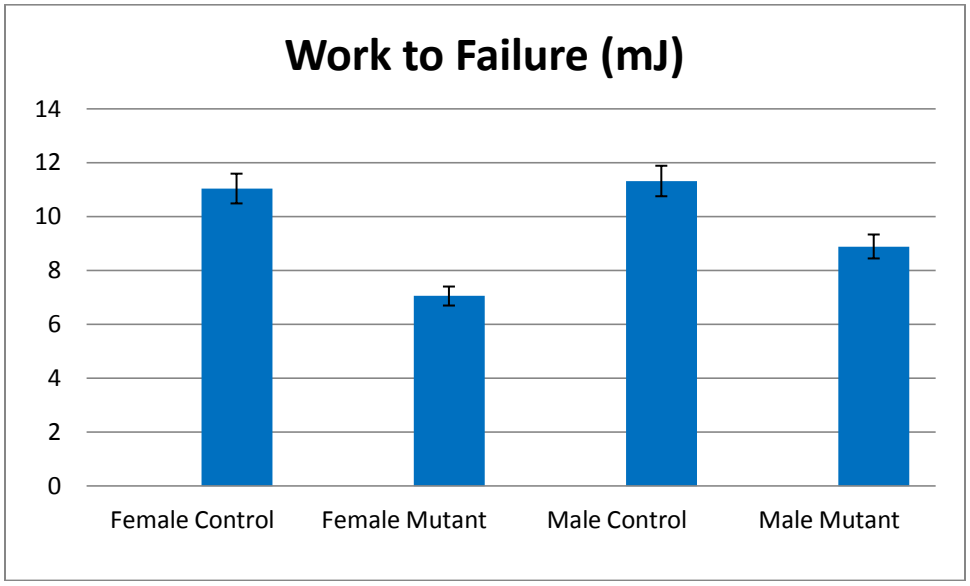

Figure 14: Comparison of work to failure.

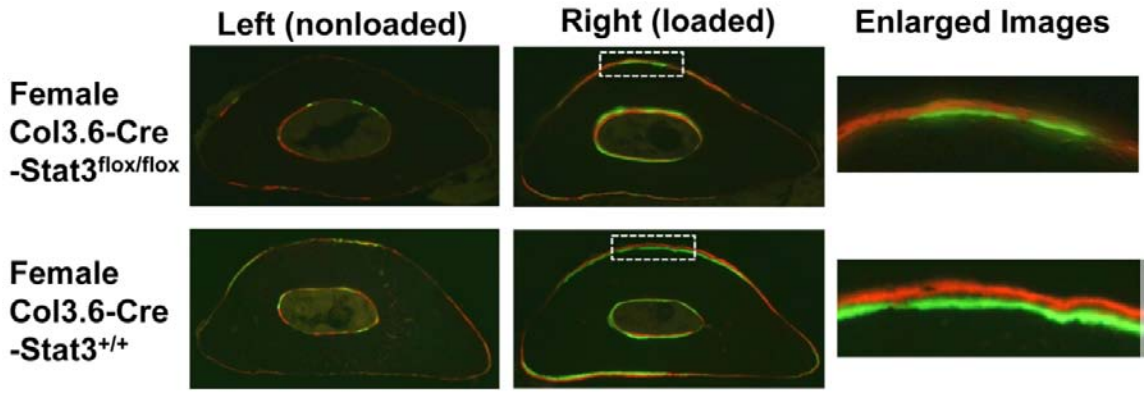

Figure 15: Comparison of midshaft ulnar sections.

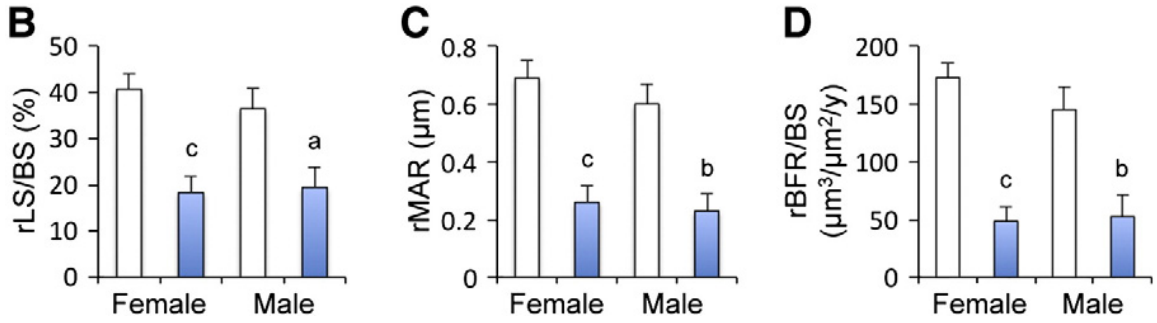

Figure 16: rMS/BS, rMAR, rBFR/BS.

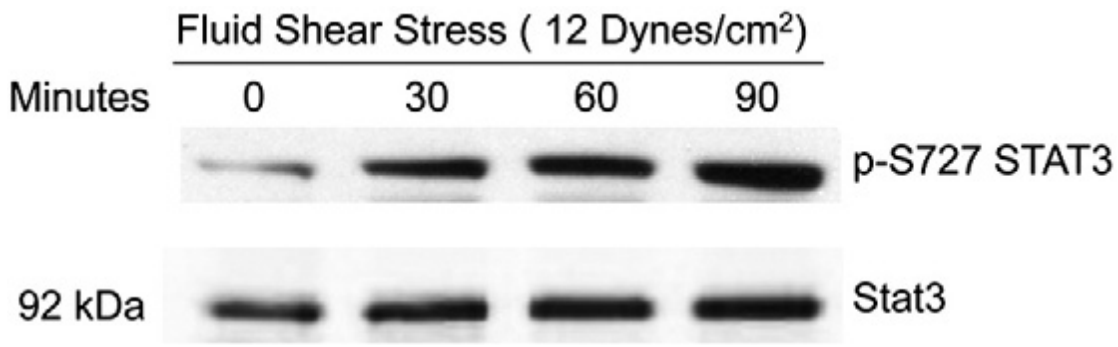

Figure 17: Serine phosphorylation of STAT3 in response to FSS.

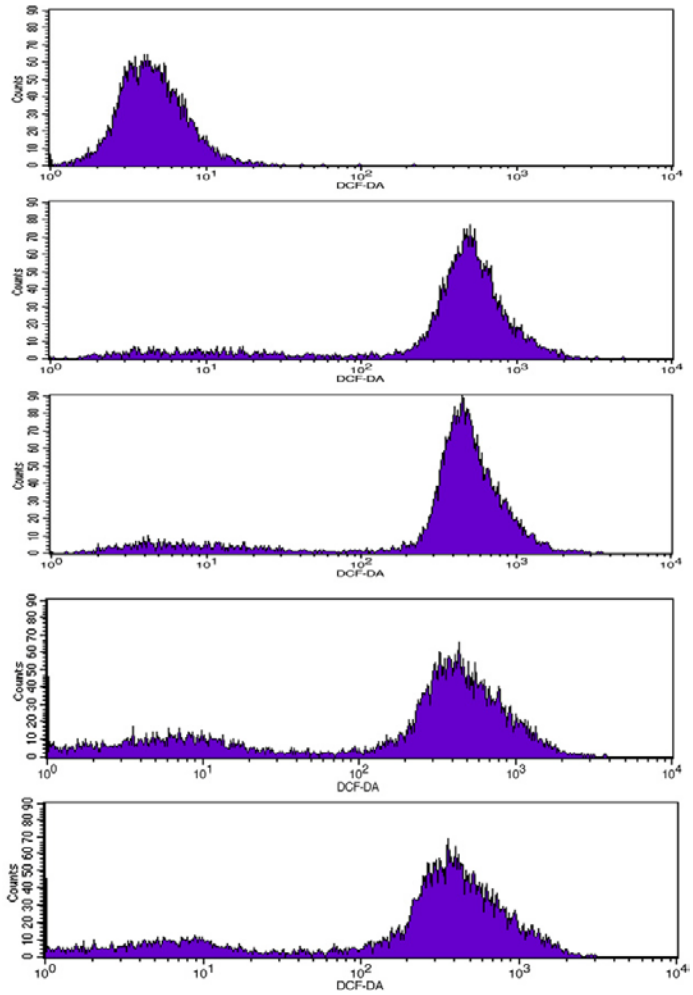

Figure 18: Flow cytometric analysis of ROS level.

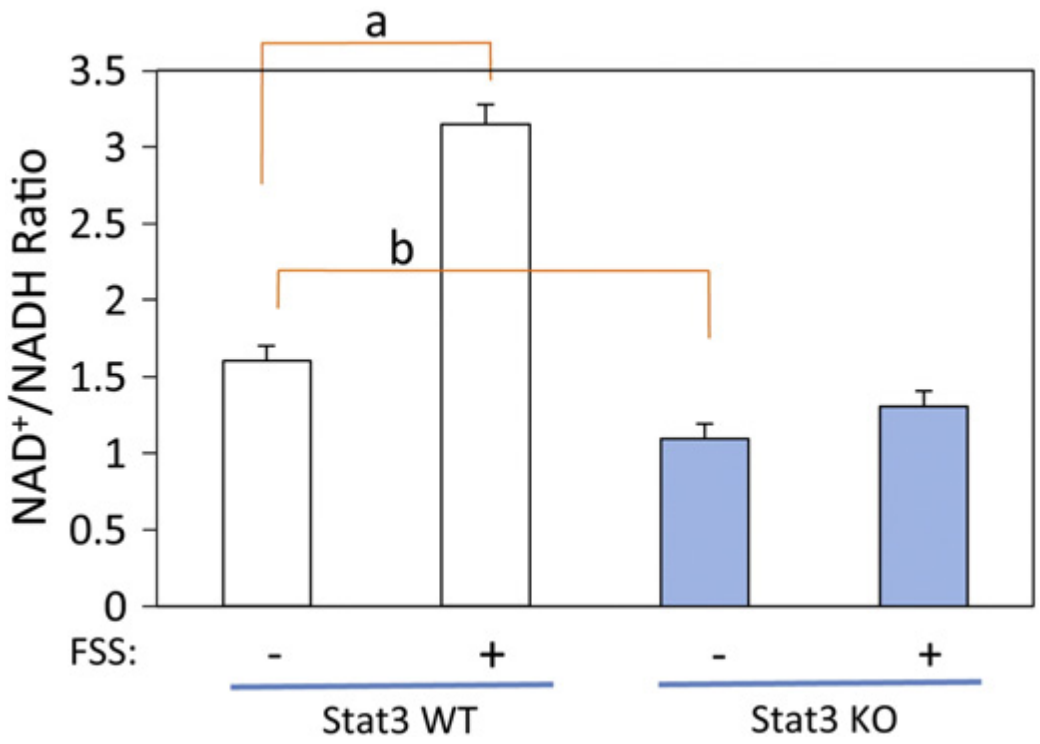

Figure 19: NAD^+/NADH ratios.

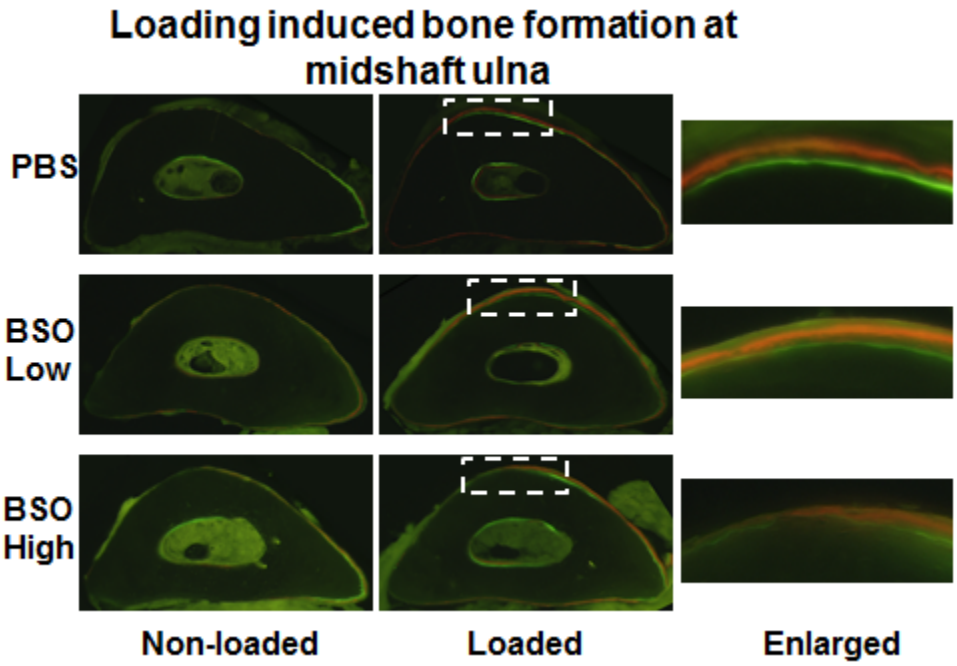

Figure 20: Midshaft ulnar sections – BSO versus control.

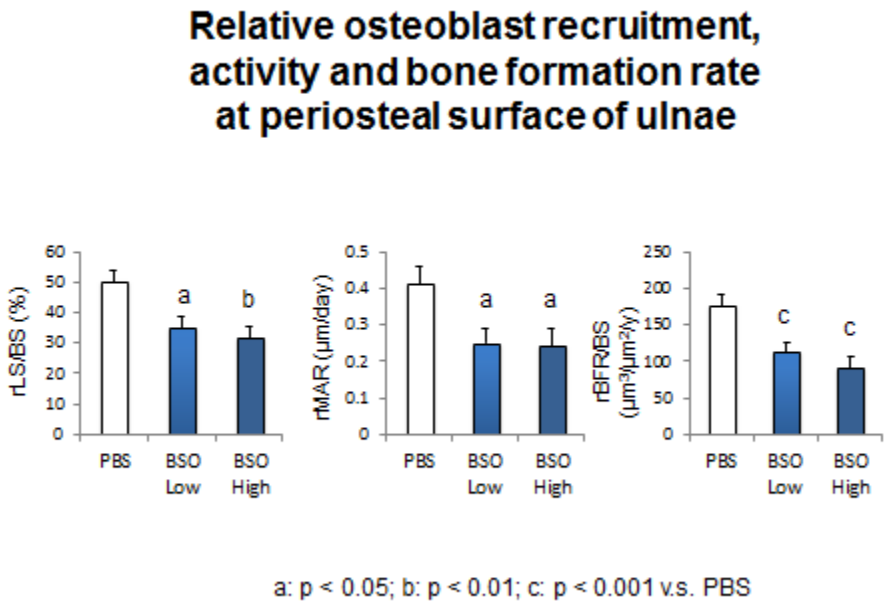

Figure 21: rMS/BS, rMAR, rBFR/BS – BSO versus control.